6.5-GHz Brain Stimulation System Using Enhanced Probe Focusing and Switch-Driven Modulation

Seongwoog Oh, *Graduate Student Member, IEEE*, Dahee Jung, Taeyoon Seo, *Member, IEEE*, Yeowool Huh, Jeiwon Cho, and Jungsuek Oh, *Senior Member, IEEE*

***Abstract*— This article, for the first time, presents the design, fabrication, and measurement results of a novel microwave brain stimulation system enabling efficient probe focusing of rectangular-pulse enveloped 6.5-GHz waves. While the conventional ON/OFF stimulation systems in literature employ low frequencies below 0.5 GHz, the proposed system employs 6.5 GHz that can achieve more spatial energy focusing and a moderate level of energy penetration depth. In the proposed system, the ON/OFF modulated microwave signal is generated by a single chip consisting of a voltage-controlled oscillator (VCO) and power amplifier (PA). The VCO is driven by a switch at the current source to generate modulated signals with over 20-dB isolation between the high and low states. The probe with a center-opened aperture surrounded by a symmetric loading enables low power reflection toward the brain and focuses the field in the square-shaped aperture of 1-mm^2 area. Finally, it is demonstrated that the 20-min stimulation of an *in vivo* mouse brain using microwave signals with 1-Hz repetitive pulse envelopes and 1% duty cycle enables the normalized firing rate to reach up to 0.2 while the normalized firing rate stays just within ±0.05 under no stimulation. This suggests that the proposed brain stimulation system can achieve a dramatic change in the activity of individual hippocampal neurons.**

***Index Terms*— Brain stimulation system, microwave circuits, neural probe, neuromodulation, probes, stimulation system.**

I. Introduction

DIVERSE brain stimulation techniques have been used to modulate brain activities during clinical and basic research [1]–[4]. In particular, brain stimulation methods using electrical and magnetic components have become increasingly popular over the past decades, and their effects on neural circuits and behaviors have been intensively investigated [3], [5]–[7]. Conventionally there are several different ways to stimulate the brain. Deep brain stimulation, for example, is an invasive stimulation method in which electric current passes through electrodes at specific parts of the brain for neuromodulation. Transcranial magnetic stimulation (TMS) [7]–[9] and transcranial direct current stimulation (tDCS) [10], [11], on the other hand, are typical noninvasive brain stimulation methods. The effects of brain stimulation on neural excitability can be separated into immediate and long-term changes. Immediate effects show when the stimulation is applied, while long-term effects observed after stimulation require several minutes of stimulation to develop [12]. Beyond simply experimenting immediate effects, recently, research into the long-term effects of deep brain stimulation, tDCS, and TMS is increasing [13]–[15]. The conventional noninvasive brain stimulation methods have both advantages and disadvantages. For instance, tDCS is less expensive than TMS [16], [17], but it is a relatively primitive technique compared to TMS. It is inefficient because approximately half of the dc current flows out through the scalp [18], it has difficulty in focusing the stimulation location, and it causes more skin irritation than TMS. Despite the advantages of TMS over tDCS, TMS also has disadvantages of high cost, lack of portability, and disturbing acoustic noise [17]. The induced current for stimulation requires a magnetic field as much as several tesla, which entails high power consumption for TMS. The coil used to focus the stimulating effects to a small area in TMS can also form a strong magnetic field around the wing of the coil, thereby unintentionally activating nontarget areas [19]. Prior evidence has shown that such electromagnetic fields directly affect the biological system, causing temperature increases, molecular signaling, and interactions with the nerves [20]. Recently, new brain stimulation techniques have been developed to treat neurological and psychiatric disorders more efficiently [21], [22]. However, the frequencies of the signals used in these techniques still cause long penetration depth and lack the ability to limit stimulation to a specific location.

Changes in the amplitudes of microwave signals have been reported to induce changes in brain activity [23], [24]. Recently, the effects of electromagnetic radiation on brain tissues at microwave frequencies that are considerably

Manuscript received December 23, 2020; revised February 26, 2021; accepted April 3, 2021. Date of publication May 10, 2021; date of current version September 2, 2021. This work was supported in part by the Creative-Pioneering Researchers Program of Seoul National University (SNU), in part by the Brain Research Program through the National Foundation of Korea (NRF) funded by the Ministry of Science, ICT & Future Planning under Grant NRF-2015M3C7A1028393, and in part by the Brain Science Research Program under Grant NRF-2015M3C7A1028392 and Grant NRF2018M3C7A1024736. *(Corresponding author: Jungsuek Oh.)*

Seongwoog Oh and Jungsuek Oh are with the Department of Electrical and Computer Engineering (ECE), Institute of New Media and Communications (INMC), Seoul National University, Seoul 151-742, Republic of Korea (e-mail: jungsuek@snu.ac.kr).

Dahee Jung is with the Center for Functional Connectomics, Korea Institute of Science and Technology, Seoul 02792, Republic of Korea.

Taeyoon Seo is with Samsung Electronics Company Ltd., Suwon 16677, Republic of Korea.

Yeowool Huh is with the Translational Brain Research Center, Catholic Kwandong University International St. Mary's Hospital, Incheon 21431, Republic of Korea, and also with the Department of Medicine, College of Medicine, Catholic Kwandong University, Gangneung-si 25601, Republic of Korea.

Jeiwon Cho is with the Department of Brain and Cognitive Science, Scranton College, Ewha Womans University, Seoul 03760, Republic of Korea.

Color versions of one or more figures in this article are available at https://doi.org/10.1109/TMTT.2021.3075726.

Digital Object Identifier 10.1109/TMTT.2021.3075726

higher than the prior brain stimulation frequencies, has been investigated [25]. Accordingly, the mechanism of neuromodulation excited by microwave brain stimulation, has been reported [26]. While 6.5 GHz, such high frequencies, are desired to improve spatial energy focusing, a modulated envelop signal generated by switching 6.5-GHz waves can enhance stimulation effects on brain tissues since neurons act as low-pass filters [27] similar to repetitive transcranial magnetic stimulation (rTMS) changes cortical excitability [11]. Conventional amplitude modulation methods using a switch at the signal path have low isolation below 20 dB between the ON and OFF states, which can generate unintended effects. Planar open-ended coaxial structures have been used for probes for biological application at microwave frequencies [28]–[30]. In the conventional design, the target frequency determines the aperture shape and size of the open-ended coaxial structure. Practically, the intended measurement area limits the shape and size of the probe, which degrades frequency responses such as the reflection coefficient at the target frequency. In addition, the aperture size must be fixed to stimulate a specified area and avoid undesired stimulation in other regions. Since the conventional probe was designed to measure the permittivity of biological materials, the reflection coefficient is typically quite high. $S_{11} < -10$ dB toward the probe input is utilized as the desired criterion. So far, no studies have measured both immediate and long-term change to brain using microwave signals simultaneously.

In this article, to confirm the effect over a long-term and immediate response, a novel 6.5 GHz focused brain stimulation system using enhanced probe focusing and switch-driven modulation is proposed to solve the aforementioned issues. Microwaves generated at 6.5 GHz are used to narrow the stimulation area, since the penetration depth into biological tissue is shortened at such frequencies. In addition, a center-opened aperture with a looped stub is proposed as the probe topology to match the biological material constituting a mouse brain at 50 Ω, thereby further focusing the field distribution. The complete system can be fabricated using a semiconductor process and printed circuit board (PCB) technology for low cost, low power, and portability.

II. Design of Stimulation System

A. Brain Modeling

The mouse brain was modeled as depicted in Fig. 1, being simulated by a full-wave electromagnetic simulator (CST Microwave Studio Suite 2018). This model only consists of the brain and skull due to the skin resection on the probe attachment to the mouse head. It should be noted that the measured brain permittivity and CST reference permittivity of the skull were applied in the model. The brain permittivity was measured using a conventional permittivity measurement probe [30]. By measuring S_{11} of reference materials such as air, distilled water, ethanol, and a mouse brain, the frequency dispersed permittivity can be calculated to be $36.3 + \text{j}\cdot 13.7$ at 6.5 GHz. For simplicity, the mouse brain was assumed to be a homogenous material and modeled as a sphere of 10-mm radius and the skull was modeled as a spherical shell of 0.2-mm thickness. The top of the model was flattened as a circle of 0.5-mm radius to consider actual contact, rendering a flat boundary between the brain model and probe.

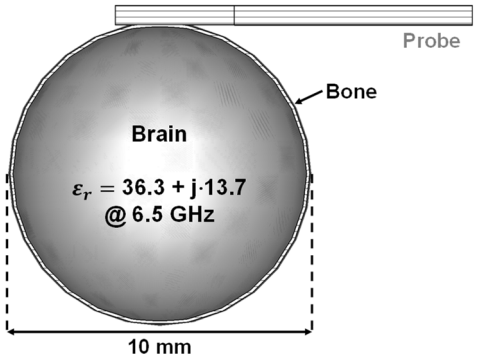

Fig. 1. Simplified mouse brain stimulation environment when the stimulation probe is on the brain model.

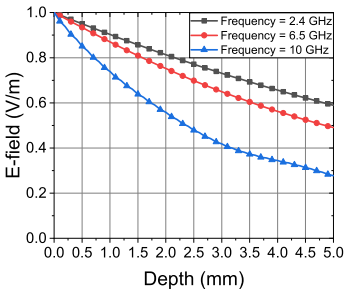

Fig. 2. Simulated E-field attenuation in the brain model for frequencies of 2.4, 6.5, and 10 GHz.

B. Stimulation Signal Generation

In general, it is known that the loss in bio-tissue in the microwave frequency band is large, so selection of an appropriate frequency is required. For frequencies of 2.4, 6.5, and 10 GHz, changes in E-field intensity with depth of a brain model is simulated and normalized as shown in Fig. 2. At 1-mm depth, for 10 GHz it shows a decrease of 27% as E-field of 0.73, while for 2.4 and 6.5 GHz it shows a decrease of 10% and 13%, respectively. In the case of a probe with a resonant structure fabricated based on a PCB, the higher the frequency leads to smaller size [31]. Therefore, a frequency of 6.5 GHz was chosen that adequately satisfies the tradeoff in the size of the overall system and attenuation.

A 6.5-GHz brain stimulation system was implemented to demonstrate the feasibility of brain stimulation using modulated microwave signals. The frequency of 6.5 GHz, which is higher than the frequencies used in prior works, was selected to achieve more focused stimulation. Stimulation signal with small guided wavelength can be focused in a small area (<1 mm^2) and stimulate only surface region (<1-mm depth). Fig. 3 shows an overall block diagram of the proposed brain stimulation system consisting of a switch-driven voltage-controlled oscillator (VCO), buffers, a power amplifier (PA), a transformer, and a stimulation probe with a center-opened aperture. When the integrated circuits are separately fabricated and connected by bonding wires,

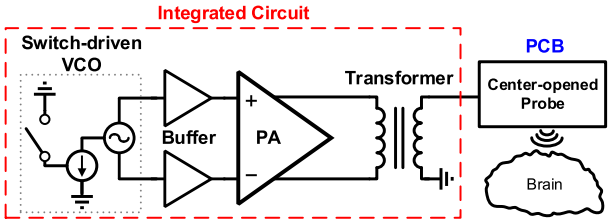

Fig. 3. Block diagram of the proposed microwave brain stimulation system.

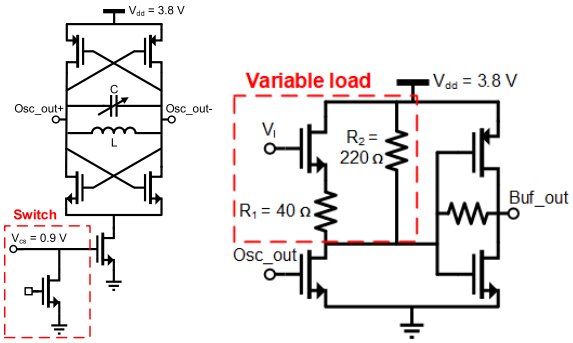

Fig. 4. (a) Schematic of switch-driven VCO and (b) buffer for output power control with variable load and isolation between VCO and PA.

the performance of the system is degraded and unpredictable due to the inaccurate inductance of the bonding wire. To solve this problem and facilitate integration, the switch-driven VCO, buffer amplifier, PA, and transformer were integrated onto a single chip.

The VCO, the microwave signal source, generates a 6.5-GHz microwave signal. A schematic drawing of the switch-driven VCO is provided in Fig. 4(a). The VCO is designed with a widely adopted n-type metal oxide semiconductor (MOS) and p-type MOS cross-coupled structure [32]. The output frequency of the oscillator is determined by the resonant frequency of the *LC* tank in the load and tuned by adjusting the varactor capacitance C in Fig. 4(a). Since the signal modulation is necessary because the neuron cell acts as a low-pass filter, a switch-driven VCO is proposed in which a switch is applied to the current source transistor in the VCO to generate the modulated signal. The switch controls the gate bias of the current source transistor and makes the VCO turn on and off, leading to high isolation of the amplitude modulation. In addition, the conventional method in which the switch is connected to the output node of the VCO causes power degradation due to the large parasitic capacitance effect of the switch at microwave frequencies, which becomes larger when the number of switches is increased to support complicated modulation. However, the switch-driven VCO has no power degradation due to control of the current source, which is connected to the virtual ground of the circuit. Furthermore, no additional power degradation occurs when the number of switches is increased.

The buffer amplifier is used to prevent the *LC* resonance frequency from changing due to variations in the impedance at the VCO output. The buffer amplifier consists of a variable load, allowing control of the output power of the entire system. Power control should be possible by observing the stimulation effects according to the power level of the stimulus signal and finding the minimum power that causes the stimulation effect. Fig. 4(b) shows a schematic of the buffer amplifier with the variable load. The loads of the common source include resistors R_1 and R_2 and a transistor, which operates as a variable resistor. When the gate voltage of the transistor, V_l is close to drain voltage, the transistor is turned on and the ON-resistance becomes very small so that the equivalent resistance becomes $R_1 \parallel R_2$. When the gate voltage reaches zero, the transistor is turned off and the value of R_2 is observed. Consequently, the gate voltage of the transistor determines the load impedance between R_2 and $R_1 \parallel R_2$. The total output power is controlled by changing the load impedance of the common source amplifier.

Since brain cells are vulnerable to elevations of temperature, the maximum power of microwave signal is adjusted to 20 dBm by adding the PA. According to our simulation results, the designed switch-driven VCO with a buffer generates the maximum output power near 0 dBm. Thus, the PA must amplify the microwave signal by 20 dB. Considering the maximum available gain of the 0.28 μm silicon on insulator (SOI) complementary MOS (CMOS) field effect transistor at 6.5 GHz, the two-stage design approach was adopted. The cascade structure is used to hold a drain voltage of 3.8 V for output powers greater than 20 dBm. In addition, transistor C_{gs} reduction is used to overcome the breakdown voltage of the transistor [33] to ensure safe operation. A schematic of the PA is shown in Fig. 5, where a differential structure is used to avoid source degeneration, which generally degrades the performance of the PA. At the output of the main stage, a varactor is applied to adjust the load matching. Since the microwave stimulation signal should be delivered to the biological material through a single-ended probe, a transformer is employed to convert the differential signal of the PA into a single-ended signal. To minimize the use of bonding wires, the transformer is integrated into a chip. The lateral coupling structure is used, considering the current capability of the metal layer. The integrated transformer, which has a 1-to-2 ratio to alleviate the control of impedance matching of the PA. Through optimization of the transformer, the size of the secondary coil was determined to be 0.18 mm $\times$ 0.18 mm, which greatly reduces the total size of the system due to integration.

C. Design and Characterization of the Proposed Probe

A novel probing topology with a center-opened aperture surrounded by symmetric loading is proposed. As shown in Fig. 6(a), the open-ended planar coaxial aperture of the conventional probe attached to the brain model makes a ring-shaped stimulation area, which suggests fields distributed along the ring-shaped open aperture, and is fed from the center. The ring-shaped stimulation area prohibits the specification of an accurate stimulation point due to the low field intensity at the center. On the other hand, the proposed

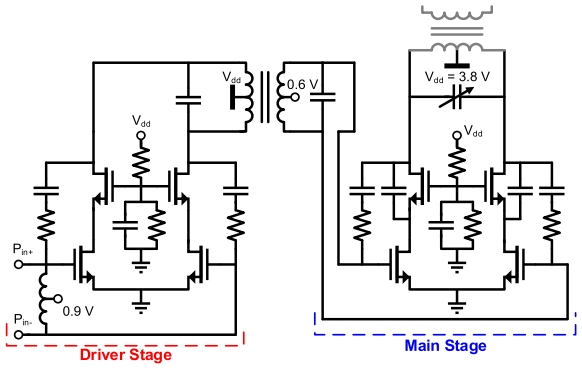

Fig. 5. Schematic of two-stage and two-stacked PA.

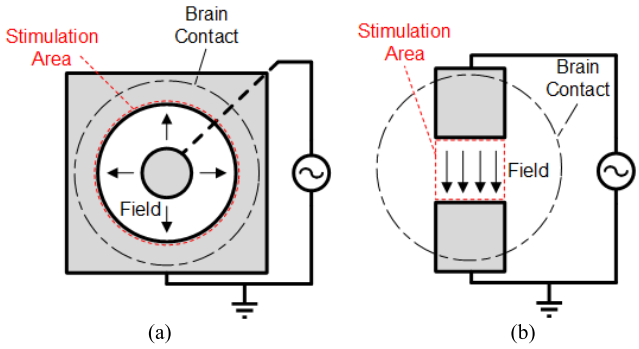

Fig. 6. Field distributions at the probe aperture with (a) planar open-ended coaxial (conventional) and (b) center-opened aperture formed by two metallic patches (proposed).

center-opened aperture with two metallic patches produces a square-shaped stimulation area, which can structurally include a target point, as illustrated in Fig. 6(b). This allows for greater focusing and equal distribution of the stimulation field on the target region under the square-shaped stimulation area. Fig. 7(a) and (b) present oblique views of the proposed probe at the top and bottom. The probe consists of a top metal, a substrate, a bottom metal, and metallic via holes, as shown in Fig. 7(c). At the top metal, a U-shaped ground and feed line are applied to attach the right-angle mount-type sub-miniature push-on (SMP) connector. It should be noted that when a conventional subminiature version A (SMA) connector is used, the signal cable connected to the SMA connector has physical interference with the mouse body. To mitigate this undesired effect, a right-angle mount-type SMP connector was chosen. The largest metallic via in Fig. 7(c) is used to feed microwave signals from the SMP connector to the proposed center-opened aperture formed by the symmetric looped stub. The other vias are used to equalize the potential between the top and bottom ground metals.

Fig. 8(a) shows the center-opened aperture formed by the two metallic patches contacting the brain model. The brain-contact patches are connected to the top feed patches through metallic vias. To characterize the variations of the input impedance, the stimulation area was fixed to be 1 mm × 1 mm. In Fig. 8(b), the impedance varies from 17.7 − j·5.1 Ω to 21.6 + j·9.44 Ω when the length of the patch is changed from 1 to 5 mm. The center-opened aperture shows a

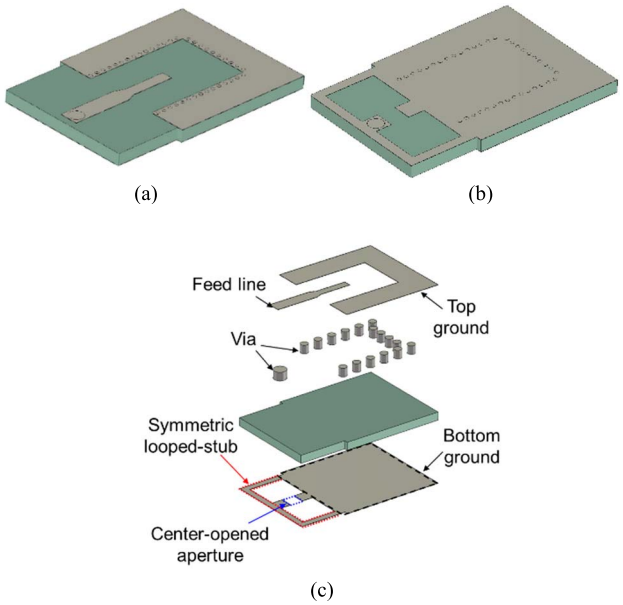

Fig. 7. Oblique views of the (a) top, (b) bottom, and (c) partially exploded view of the proposed probe. The feed structure is added to the center-opened aperture surrounded by the symmetric looped stub.

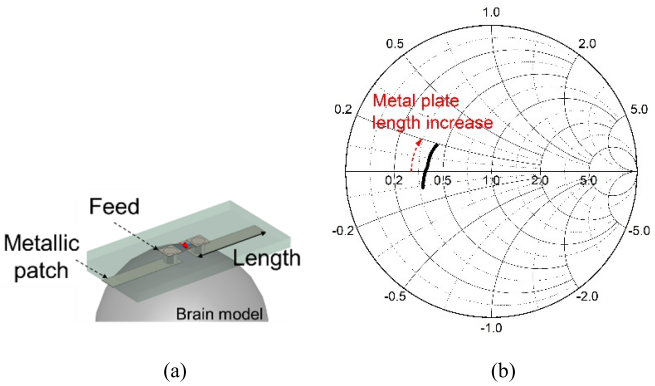

Fig. 8. (a) Proposed probe with a center-opened aperture and (b) impedance variation on a Smith chart as a function of the length of each metallic patch when contacting the brain model.

6.5-GHz resonant frequency corresponding to a patch length of 1.6 mm, where the input impedance becomes purely real as 18.9 Ω. The return loss of the proposed structure was observed to be 6.9 dB, which is still low and thus lowers the power efficiency of the brain stimulation system.

As discussed in Section I, a high return loss is essential to achieve efficient power delivery to the brain model. Fig. 9(a) is a simplified diagram of the environment in which the probe is in contact with the brain. ε_1 and ε_2 are the permittivities of the probe substrate and the mouse brain, respectively. w, t, and g are the width, thickness, and spacing of the metal line. For the additional capacitance caused by the fringing field, the capacitance formula was derived considering the different dielectrics that exist above and below the metal line. Referring to [34] and [35], the capacitance caused by the metal gap of the proposed probe was obtained as follows:

$$C_g = (\varepsilon_1 + \varepsilon_2)\frac{t}{2g}\left[1 + \frac{g}{\pi t}\ln\left(\frac{\pi t}{2g}\right)\right]. \quad (1)$$

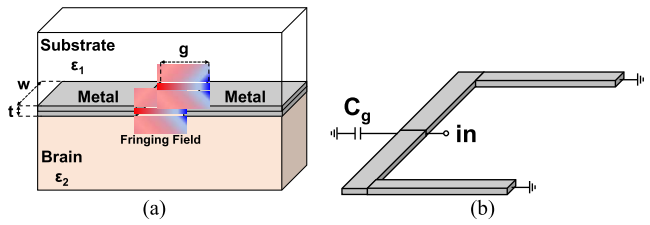

Fig. 9. Simplified diagram of the (a) structural capacitance and (b) inductance of the proposed probe.

Fig. 9(b) is a diagram of grounded shunt stubs connected to C_g, a capacitor formed by a metal gap. Since the structure of the diagram has symmetrical stubs, the equivalent inductance is half of each stub inductance. The inductance of the grounded shunt stub can be expressed as [36]

$$L_S(\text{nH}) = 2\times 10^{-4}\cdot l\left[\ln\left(\frac{l}{w+t}\right)+1.193+0.2235\cdot\frac{w+t}{l}\right]\cdot K_g \tag{2}$$

$$K_g = 0.57 - 0.145\cdot\ln\frac{w}{h} \tag{3}$$

where K_g, w, t, and l are the correction factor, width, thickness, and total length. According to our heuristic studies considering the brain model, the initially designed aperture structure consisting of only two metallic patches is lacking in control of the real part of the input impedance while maintaining an imaginary part of zero. In this sense, it is proposed to place a looped stub around the two metallic patches as reactive control loading to achieve a low reflection coefficient toward the brain model, as illustrated in Fig. 10(a). The equivalent circuit of the center-opened aperture formed by a looped stub can be expressed as a combined series and parallel *LC* resonators, as shown in Fig. 10(b). The input impedance and resonant frequency of the focusing center-opened aperture in cooperation with the proposed reactive loading can be expressed using (4) and (5), as shown at the bottom of the next page.

where L_s and L_v are the inductances of the stub and via, respectively. C is the sum of the capacitances of the two patches and the parasitic capacitance of the stub. R_b is the loss factor of the brain model at microwave frequencies. Changing the dimensions of the stub affects the values of C and L_s in (5), and thus many combinations of C and L_s can be employed to achieve a specific resonant frequency. Consequently, the real term of the impedance Z_{mtch} in (4) can be varied by choosing adequate stub dimensions while maintaining resonance at 6.5 GHz, as shown in Fig. 10(c). Finally, it was found that Z_{mtch} could be controlled to be 45.3 Ω near 50 Ω at 6.5 GHz when the length and width of looped stub were chosen to be 11 and 11.3 mm, respectively.

The field distributions at the aperture were simulated using an injected power of 10 mW. A single looped stub forms a nonuniform and asymmetric stimulation area, while the desired uniform field distribution can be obtained by applying the proposed symmetric looped stub, as depicted in Fig. 11. Since the area of the field is confined only between the gaps, the proposed probe has a stimulus area in square millimeters.

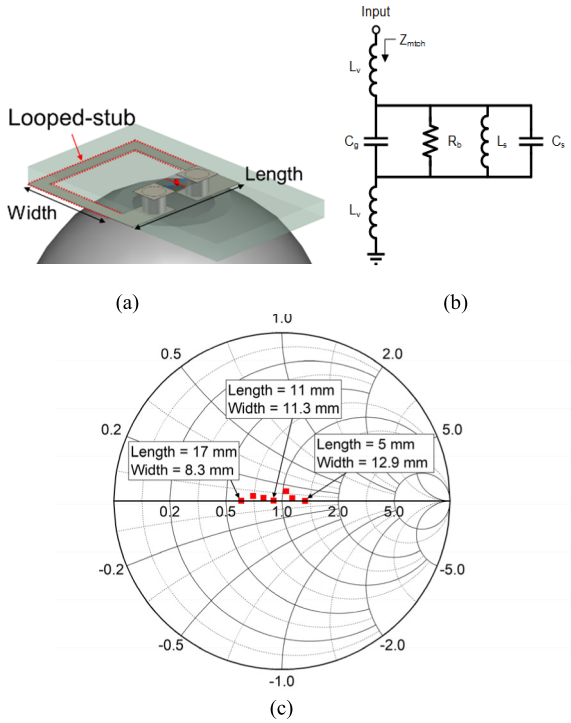

Fig. 10. (a) Schematic, (b) equivalent circuit, and (c) input impedances for the various dimensions of the looped stub surrounding the center-opened aperture contacting the brain model.

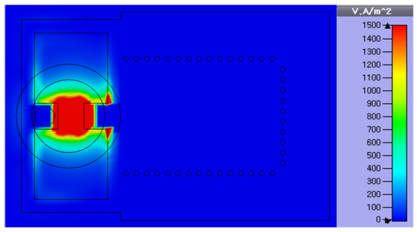

Fig. 11. Simulated field distributions for symmetric looped stub applied probes.

The probe is manufactured through a general PCB process without any additional processing and is designed to comply with the regulations of a minimum linewidth of 100 μm, a gap of 100 μm, and via diameter of 200 μm. Mismatch effects are simulation by applying the variation of 50–100 μm, the maximum error range of the linewidth that can be occurred during the PCB fabrication, is applied in the transmission line and stub width of the probe as shown in Fig. 12. The width of the transmission line and stub varied in the range of 0.9–1.1 and 0.4–0.6 mm, respectively. Generally, when the linewidth decreases, the mutual inductance increases, but the parasitic capacitance of the line decreases due to the area reduction. Since the matching of the probe is based on the resonance of the inductor-capacitor, as a result, the increase in inductance and the decrease in capacitance are canceled out and the resonance frequency remains unchanged.

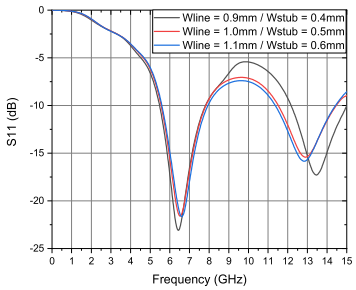

Fig. 12. Simulated S_{11} of probe according to 100-μm width mismatches.

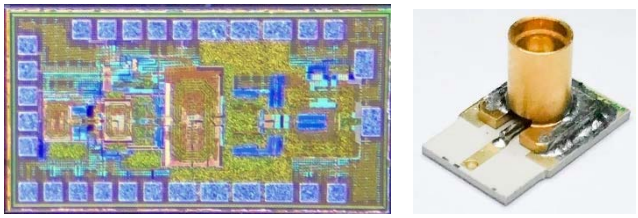

(a) (b)

Fig. 13. Photographs of (a) switch-modulated microwave generator integrated circuit and (b) fabricated brain model-matched probe.

III. Implementation and Measurement of the Proposed Brain Stimulation System

A. Microwave Stimulation System

Fig. 13(a) provides a photograph of the fabricated integrated chip for generating a switch-modulated microwave signal. An integrated chip was fabricated using a 0.28-μm SOI CMOS process. The dimensions of the entire chip were 1.38 mm $\times$ 0.91 mm, and it was mounted on a 30 mm $\times$ 30 mm module. The measurement bias of the IC was 3.8 V. The designed brain model-matched probe was fabricated using PCB technology considering cost effectiveness. The length of the looped stub was chosen to be 6 mm, and the total dimensions of the probe were 11.8 mm $\times$ 8 mm. An RO/Duroid 3010 (Rogers Corp.) with a high dielectric constant ($\varepsilon_r = 10.2$) was selected to minimize the probe dimensions for the small size of the mouse brain, and a thickness of 0.635 mm was used for rigidness and tight attachment to the surface of the brain. Fig. 13(b) shows a photograph of the fabricated probe.

Fig. 14 compares the simulated S-parameter and power density inside the brain model at a depth of 0.4 mm between the conventional open-ended coaxial probe and the proposed probe when the injected power was 10 mW. The excited power density inside the brain must be correlated with S_{11}, and thus S_{11} must be low for high power density inside the brain model. Using the proposed probe, the power density

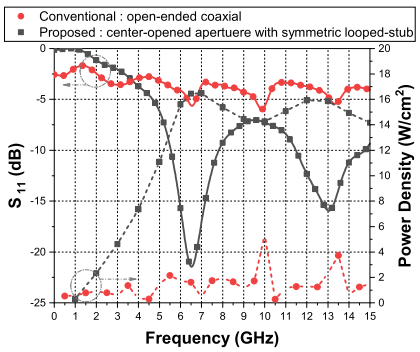

Fig. 14. Comparison between conventional and proposed probing topologies in simulated S_{11} and power density inside the brain model at a depth of 0.4 mm.

can be improved from 1.62 to 16.4 mW, and S_{11} is improved from -6.1 dB (25% reflection) to -21.4 dB (0.7% reflection) at 6.5 GHz. These results suggest that the proposed probe requires ten times less power to achieve the same power density inside the brain. Fig. 15(a) and (b) compare the simulated and measured S_{11} of the proposed probe when the center-opened aperture was in contact with the air, distilled water, and the mouse brain. In Fig. 15(a), the return loss is 0.27 dB at 6.5 GHz when the probe is not in contact with any material, only the air. On the contrary, when the proposed probe with a center-opened aperture is in contact with distilled water, the return loss increases to 11.2 dB. Fig. 15(b) shows that S_{11} was measured to be less than -10 dB in the range of 6.1–7.7 GHz, where S_{11} is -13.2 dB at 6.5 GHz. Linking the measured values of S_{11} in Fig. 15(b) to the simulated power density in Fig. 14, the probe demonstrates enhanced power efficiency at 6.5 GHz.

The measured output signals of the microwave signal generator chip are compared in Table I along with other state-of-the-art VCO and PA operating in similar frequency. The chip was turned on with 3.8-V drain bias and consumed a dc current of 350 mA. The frequency was tuned between 5.7 and 7.12 GHz, changing the varactor voltage in the VCO from 1.2 to 5 V. With the modulation switch turned off, the output power varies from 3.2 to 22.4 dBm at 6.5 GHz. The variable load voltage in the buffer changes from 0.6 to 5 V. Fig. 16 also confirms that the continuous signal was modulated when rectangular pulses were applied to the system. Rectangular pulses with a 1-MHz pulse frequency and 50% duty cycle were used as the stimulation protocol. When the protocol was applied, the average power consumption of the signal was reduced by 3 dB (50%) compared to when a continuous signal was employed. The pulse-enveloped signal has more than 20-dB isolation between the ON and OFF

$$Z_{\text{mtch}} = \frac{\omega^2 R_b L_s^2}{(R_b - \omega^2 R_b C L_s)^2 + \omega^2 L_s^2} + j\omega \frac{2R_b^2 C^2 L_s^2 L_v \omega^4 + (2L_s^2 L_v - 4R_b^2 C L_s L_v - R_b^2 C L_s^2)\omega^2 + 2R_b^2 L_v + R^2 L_s}{(R_b - R_b C L_s \omega^2)^2 + L_s^2 \omega^2} \tag{4}$$

$$\omega_r^2 = \frac{4R_b^2 C L_v + R^2 C L_s - 2L_s L_v}{4R_b^2 C^2 L_s L_v} \pm \frac{\sqrt{R_b^4 C^2 L_s^2 + 4L_s^2 L_v^2 - 16R_b^2 C L_s L_v^2 - 4R_b^2 C L_s^2 L_v}}{4R_b^2 C^2 L_s L_v} \tag{5}$$

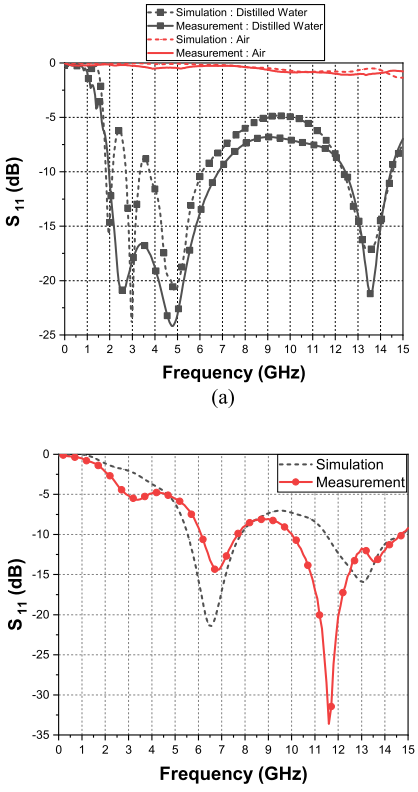

Fig. 15. Simulated and measured S_{11} of the proposed probe when the center-opened aperture was in contact with the (a) air and distilled water and (b) mouse brain.

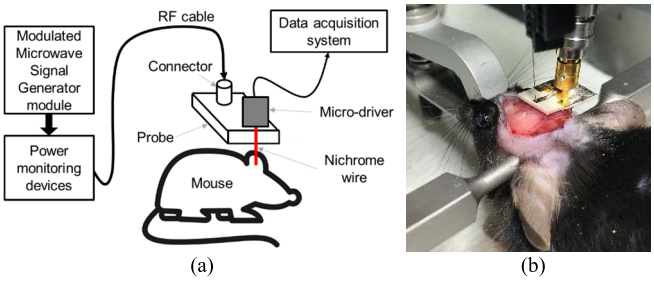

Fig. 16. (a) Experimental setup consisting of the proposed modulated microwave signal generator and a probe and (b) photograph of the stimulation probe and nichrome wires of a microdrive.

states. While the clinical stimulation protocols of rTMS or theta burst stimulation (TBS) typically use frequencies less than 100 Hz, the proposed brain stimulation system generates stimulus signals over a wide frequency range up to 1 MHz, including the stimulation protocols used for rTMS and TBS.

B. Animal Experiments

Mice were used to validate the feasibility of the proposed brain stimulation system. First generations of male hybrid mice of C57BL/6JúI129/SvJae (more than 8-weeks old) were used in both a single-unit recording experiment and a temperature measurement experiment. The mice were housed under an alternating 12-h light/dark cycle (lights on at 9 AM) and had free access to food and water. The experimental protocols for the animal study were approved by the Institutional Animal Care and Use Committee of the Korea Institute of Science and Technology (Approval Number: 2015019). The experimental setup with the proposed stimulation system and probe is shown in Fig. 16(a). We connected a commercial power monitoring device between the system and an probe to measure the signal power. Two pairs of couplers (158020, Krytar) and a power meter (E4417A, Agilent) were used to separate the incident and reflected powers, and an isolator (DMI6018, DiTom Microwave) was employed to isolate them. The detailed settings used to measure the incident and reflected powers can be found in [41]. By measuring the incident and reflected powers, the power delivered from the probe to the brain was calculated. In this experiment, the average delivered power was -11.27 dBm ($= 74.6\ \mu$W), with 8.73-dBm peak power.

TABLE I
PERFORMANCE COMPARISON OF VCO AND PAS

	This Work	[34] VCO	[35] VCO	[36] PA	[37] Front-end
Process	0.28-μm SOI CMOS	0.25-μm CMOS	0.18-μm CMOS	65-nm CMOS	0.5-μm SiGe BiCMOS
Topology	VCO : LC cross-coupled PA : 2-stage differential 2 stacked	LC cross-coupled	Transformer based LC tank	2-stage differnetial 3 stacked	VCO : LC cross-coupled PA : 2-stage differential
Center Freq. (GHz)	6.41	5.25	6.45	6.5	5.49
Tuning Range (%)	22.2	24.7	9.30	N.A.	11.30
Output Power (dBm)	22.4	-5	N.A.	27.4	23
Phase Noise (dBc/Hz)	-112.05 @ 1 MHz	-117 @ 1 MHz	-122.85 @ 1 MHz	N.A.	-119 @ 1 MHz
P_{DC} (W)	1.3	N.A.	0.02	2.9	0.66
Size (mm^2)	VCO: 0.2 × 0.17 PA: 0.91 × 0.37	0.32 × 0.3	1 × 0.9	1.3 × 2.2	2.6 × 2.6

C. In Vivo Neural Signal Recording

Mice anesthetized with urethane were used to measure the effects of stimulation on the activity of individual hippocampal neurons in the brain. Four mice were used as a stimulation group to which the modulated stimulation signals were delivered. Four additional mice were used as a control group that underwent the same procedure except for the stimulation delivery. The head of each mouse was fixed with a small animal stereotaxic instrument (Kopf, USA) for precise stimulation and recording of the target brain region. After removing the skull above the target region, a stimulation probe was placed in direct contact with the brain. Then, nichrome wires of a micro-drive were inserted into the target

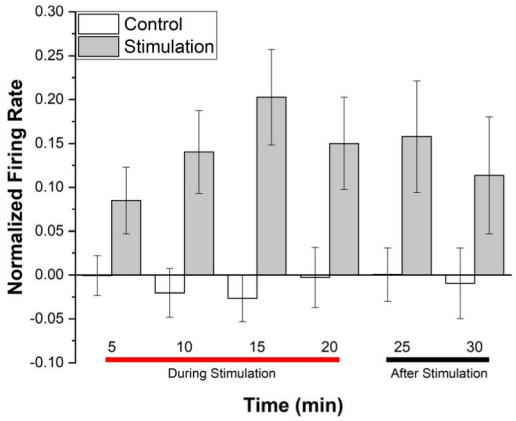

Fig. 17. Cellular response to the modulated microwave signal. A positive value indicates excitation, while a negative value indicates the inhibition of neuronal activity. Normalization was performed based on the baseline firing rate. ($N = 34$ neurons, four mice in the stimulation group; $N = 18$ neurons, four mice in the control group.)

TABLE II
NEURONAL ACTIVITY IN EACH SESSION

Session	Raw Firing Rate (Hz)		Normalized Firing Rate (Hz)	
	Control	Stim.	Control	Stim.
Baseline	0.46 ±0.069	0.40 ±0.070		
During Stimulation I First Phase (0–10 min)	0.44 ±0.074	0.46 ±0.087	-0.01 ±0.024	0.12 ±0.042
During Stimulation II First Phase (10–20 min)	0.45 ±0.078	0.53 ±0.087	0.01 ±0.029	0.18 ±0.053
After Stimulation	0.48 ±0.083	0.52 ±0.109	-0.002 ±0.033	0.15 ±0.064

brain area through a via hole in the signal line of the probe to record the electrophysiological activity of neurons in the brain [42]. Fig. 16(b) shows a photograph of a probe placed on the top of a mouse brain with nichrome wires (12 μm in diameter) to measure the neuronal activity changes induced by the microwave stimulation. The wires were mounted in a microdrive to adjust the recording depth in the brain. The nichrome wires used to record the neuronal activity, which were placed through a hollow metallic via hole in the signal line of the probe. Brain stimulation and neuronal activity recording were performed simultaneously to investigate the direct effects of the new brain stimulation method.

Microwave signals were delivered in the form of pulse envelopes (10-ms width, 1-Hz repetition). The modulation switch was operated for 10 ms and repeated every 1 s. As a result, the envelope of the microwave signal had a rectangular pulse shape with a duty cycle of 1%.

Single unit data were sorted and confirmed to be isolated from the noise through various tasks such as temporal coherence and principal component analysis (PCA) with a unique interspike interval histogram model and auto correlogram model that hippocampal neurons have. In detail, 600–6000-Hz filtering was performed and then sorted into a single neuron unit in a standardized method of tetrodes. Then, the recorded data of the CA1 pyramidal neurons in the hippocampus were used for further analysis. In total, 34 neurons from the stimulation group and 18 neurons from the control group were recorded. To assess the effects of stimulation on neuronal activity, the firing rates of the neurons were recorded for 40 min: before (10 min: baseline), during (20 min: during stimulation session, 10 ms pulse width), and after (10 min: after stimulation session) stimulation. In the control group, the first 10 min of data from the total of 40 min of recorded data were used as a baseline to measure the effects of time during the experimental procedure on the firing activity for comparison.

The effects of the modulated microwave signal on brain stimulation were observed by comparing the firing rates before (baseline), during, and after stimulation. Fig. 17 presents the resulting firing rates relative to the baseline, which were normalized using the following equation [43]:

$$\text{Normalized firing rate} = \frac{\text{firing rate in unit time-firing rate of baseline}}{\text{firing rate in unit time} + \text{firing rate of baseline}}. \quad (6)$$

Values greater than 0 indicate increased activity, while values less than 0 indicate decreased activity relative to the baseline. The error bars indicate the standard error of the mean (SEM). During the stimulation session, the stimulation group that received repetitive 1 Hz stimulation showed significantly enhanced neuronal activity as the stimulation time elapsed, whereas the control group did not show any differences. Two-way ANOVA with repeated measures; significant effect of group, $F(1, 50) = 5.718$, $P = 0.021$; significant effect of group $\times$ time interaction, $F(2.072, 103.591) = 4.384$, $P = 0.014$; no significant effect of stimulation time, $F(2.07, 103.591) = 1.978$, $P = 0.142$), as shown in Fig. 17. Waveforms of measured neural activity in the time domain are shown in Fig. 18. Neural signals contaminated by noise generated by the measurement equipment were excluded from the experimental results. The enhanced neuronal activity persisted for a short time after the stimulation was turned off (after-stimulation session). Table II summarizes the average raw data of firing rate (Hz) $\pm$ SEM and the average normalized values $\pm$ SEM relative to the baseline during each session. These results imply that the duration of stimulation is strongly correlated with the magnitude of the increase in neuronal activity (Fig. 17). Moreover, the after-stimulation session shows that the enhanced neuronal activity remained for a short time even after the stimulation ended. This finding indicates that stimulation has both immediate and lasting effects that influence neuron activity.

After confirming the effects of stimulation on neuronal activity, we investigated whether or not temperature influenced the results, since brain activity is sensitive to temperature

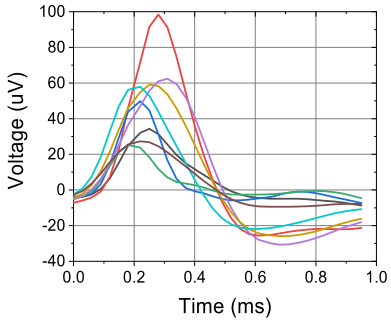

Fig. 18. Measured neural activity waveform in time domain for each cluster.

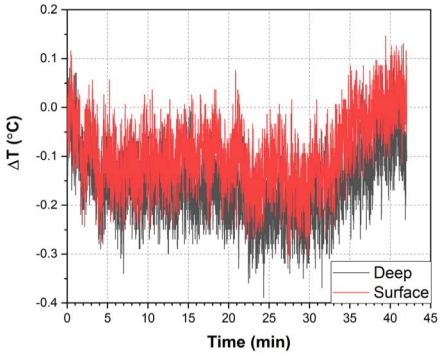

Fig. 19. Changes in temperature in the hippocampus and on the brain surface when microwave energy is delivered to the brain.

changes. An increase in brain temperature of 6–8 °C causes irreversible damage to brain tissue, and an increase by 1.5–3 °C noticeably affects neuronal activity [44]–[46]. Microwave energy generates frictional heat by rotating water molecules in the brain; this heat, if any, could have caused changes in neuronal activity. Therefore, temperature changes were measured separately before, during, and after brain stimulation. A fiber optical thermometer (m822, Luxtron), unlike a conductor thermometer that does not change the boundary conditions of the electromagnetic field, was used. The brain temperature measurement results obtained when the delivered power was equal to that of the stimulus signal revealed that no temperature changes were induced by the stimulation used in this study, as shown in Fig. 19. The temperature measured for 5 min before stimulation was averaged as a baseline temperature. Then, the temperature difference between during and after each session was calculated at each time point by comparison with the baseline temperature. The average temperature variations during and after stimulation were found to be −0.126 °C and −0.128 °C, respectively. These results confirm that the temperature changes did not cause the neuronal activity to change and strongly suggests that the electromagnetic field amplitude with the new stimulation method may have been the sole factor causing the firing rate of the neurons to increase.

IV. Conclusion

In this article, we proposed, for the first time, a 6.5-GHz focused noninvasive system to stimulate neurons in the brain using a switch-driven VCO to generate a rectangular-pulse enveloped microwave signal with a desired level of ON/OFF isolation as high as 20 dB. A microwave frequency of 6.5 GHz is chosen for its enhanced spatial focusing ability and the required penetration depth due to its small guided wavelength. A signal generator (switch-driven VCO), buffer, PA, and transformer were fabricated using a CMOS process and integrated into a single chip for generating enveloped microwave signal with low cost. The proposed probe with a center-opened aperture topology is small, lightweight, and able to boost power density in a narrow specified target area. Therefore, the proposed probe is appropriate for attachment onto the small head of a mouse to transmit and focus brain stimulation signals.

The effect of the modulated microwave signal on brain activity was evaluated by measuring the activity of individual neurons in mice. Before, during, and after stimulation, the changes in neuronal activity were measured and analyzed. The pulse enveloped signal, with 10-ms width, was delivered once per second. The stimulation increased the neuronal activity over time gradually and significantly. Finally, the effects persisted for some time after the 20-min stimulation had stopped. Our results demonstrate that modulated microwave probing with pulse envelopes is an effective and successful method of stimulating neurons. It offers several advantages over conventional brain stimulation approaches. The proposed system focuses the distribution of the electromagnetic field on a narrow region and thus the power consumption can be lowered compared to those in other studies on TMS effects using small animals. In addition, since this experiment was conducted for mice, such a small animal, a very low power level, approximately 74.6 μW, was enough to change neural activities as intended. The dc power consumption of the new stimulation method is extremely low, near 1.33 W at most, while the commercial TMS devices consume about 400 W (eXimia TMS, nexstim). The proposed stimulation probe is also easily adjustable within the given range of the stimulation area. Stimulation depth can be adjusted by optimizing the size of the probe gap, the frequency of the stimulation signal, and the power intensity. In addition, since the pulse width and repetition frequency of the stimulus signal can be adjusted easily, several different stimulation protocols, which may have different effects on neural activities, can readily be tested.

References

[1] V. Gradinaru, M. Mogri, K. R. Thompson, J. M. Henderson, and K. Deisseroth, "Optical deconstruction of parkinsonian neural circuitry," *Science*, vol. 324, no. 5925, pp. 354–359, Apr. 2009.

[2] B. D. Greenberg *et al.*, "Deep brain stimulation of the ventral internal capsule/ventral striatum for obsessive-compulsive disorder: Worldwide experience," *Mol. Psychiatry*, vol. 15, no. 1, pp. 64–79, Jan. 2010.

[3] M. Hallett, "Transcranial magnetic stimulation and the human brain," *Nature*, vol. 406, no. 6792, pp. 147–150, Jul. 2000.

[4] Y. Tufail *et al.*, "Transcranial pulsed ultrasound stimulates intact brain circuits," *Neuron*, vol. 66, no. 5, pp. 681–694, Jun. 2010.

[5] D. R. Merrill, M. Bikson, and J. G. Jefferys, "Electrical stimulation of excitable tissue: Design of efficacious and safe protocols," *J. Neurosci. Methods*, vol. 141, no. 2, pp. 171–198, Feb. 2005.

[6] M. H. Histed, V. Bonin, and R. C. Reid, "Direct activation of sparse, distributed populations of cortical neurons by electrical microstimulation," *Neuron*, vol. 63, no. 4, pp. 508–522, Aug. 2009.

[7] S. Rossi, M. Hallett, P. M. Rossini, and A. Pascual-Leone, "Safety, ethical considerations, and application guidelines for the use of transcranial magnetic stimulation in clinical practice and research," *Clin. Neurophysiol.*, vol. 120, no. 12, pp. 2008–2039, Dec. 2009.

[8] P. M. Rossini *et al.*, "Non-invasive electrical and magnetic stimulation of the brain, spinal cord, roots and peripheral nerves: Basic principles and procedures for routine clinical and research application. An updated report from an I.F.C.N. committee," *Clin. Neurophysiol.*, vol. 126, no. 6, pp. 1071–1107, Jun. 2015.

[9] P. B. Fitzgerald, S. Fountain, and Z. J. Daskalakis, "A comprehensive review of the effects of rTMS on motor cortical excitability and inhibition," *Clin. Neurophysiol.*, vol. 117, no. 12, pp. 2584–2596, Dec. 2006.

[10] M. A. Nitsche and W. Paulus, "Excitability changes induced in the human motor cortex by weak transcranial direct current stimulation," *J. Physiol.*, vol. 527, no. 3, pp. 633–639, Sep. 2000.

[11] M. A. Nitsche *et al.*, "Transcranial direct current stimulation: State of the art 2008," *Brain Stimulation*, vol. 1, no. 3, pp. 206–223, Jul. 2008.

[12] Y. Z. Huang *et al.*, "Plasticity induced by non-invasive transcranial brain stimulation: A position paper," *Clin. Neurophysiol.*, vol. 128, pp. 2318–2329, Nov. 2017.

[13] M. Alpaugh *et al.*, "A novel wireless brain stimulation device for long-term use in freely moving mice," *Sci. Rep.*, vol. 9, no. 1, pp. 1–10, Apr. 2019.

[14] C. A. Sánchez-León *et al.*, "Immediate and long-term effects of transcranial direct-current stimulation in the mouse primary somatosensory cortex," *bioRxiv*, to be published.

[15] L. De Risio *et al.*, "Recovering from depression with repetitive transcranial magnetic stimulation (rTMS): A systematic review and meta-analysis of preclinical studies," *Transl. Psychiatry*, vol. 10, no. 1, p. 393, Nov. 2020.

[16] L. C. Valiengo, I. M. Bensenor, P. A. Lotufo, R. Fraguas, and A. R. Brunoni, "Transcranial direct current stimulation and repetitive transcranial magnetic stimulation in consultation-liaison psychiatry," *Brazilian J. Med. Biol. Res.*, vol. 46, no. 10, pp. 815–908, Oct. 2013.

[17] A. Priori, M. Hallett, and J. C. Rothwell, "Repetitive transcranial magnetic stimulation or transcranial direct current stimulation?" *Brain Stimulation*, vol. 2, no. 4, pp. 241–245, Oct. 2009.

[18] P. C. Miranda, M. Lomarev, and M. Hallett, "Modeling the current distribution during transcranial direct current stimulation," *Clin. Neurophysiol.*, vol. 117, no. 7, pp. 1623–1629, Jul. 2006.

[19] H. R. Siebner, G. Hartwigsen, T. Kassuba, and J. C. Rothwell, "How does transcranial magnetic stimulation modify neuronal activity in the brain? Implications for studies of cognition," *Cortex*, vol. 45, no. 9, pp. 1035–1042, Oct. 2009.

[20] A. Rosen, M. A. Stuchly, and A. Vander Vorst, "Applications of RF/microwaves in medicine," *IEEE Trans. Microw. Theory Techn.*, vol. 50, no. 3, pp. 963–974, Mar. 2002.

[21] N. Grossman *et al.*, "Noninvasive deep brain stimulation via temporally interfering electric fields," *Cell*, vol. 169, pp. 1029–1041, Jun. 2017.

[22] H. Li, J. Sun, D. Zhang, D. Omire-Mayor, P. A. Lewin, and S. Tong, "Low-intensity (400 mW/cm^2, 500 kHz) pulsed transcranial ultrasound preconditioning may mitigate focal cerebral ischemia in rats," *Brain Stimulation*, vol. 10, no. 3, pp. 695–702, May 2017.

[23] R. C. Beason and P. Semm, "Responses of neurons to an amplitude modulated microwave stimulus," *Neurosci. Lett.*, vol. 333, no. 3, pp. 175–178, Nov. 2002.

[24] S. Roggeveen, J. van Os, and R. Lousberg, "Does the brain detect 3G mobile phone radiation peaks? An explorative in-depth analysis of an experimental study," *PLoS ONE*, vol. 10, no. 5, May 2015, Art. no. e0125390.

[25] A. Suhhova, M. Bachmann, D. Karai, J. Lass, and H. Hinrikus, "Effect of microwave radiation on human EEG at two different levels of exposure," *Bioelectromagnetics*, vol. 34, no. 4, pp. 264–274, May 2013.

[26] H. Hinrikus, M. Bachmann, and J. Lass, "Understanding physical mechanism of low-level microwave radiation effect," *Int. J. Radiat. Biol.*, vol. 94, no. 10, pp. 877–882, Oct. 2018.

[27] B. Hutcheon and Y. Yarom, "Resonance, oscillation and the intrinsic frequency preferences of neurons," *Trends Neurosci.*, vol. 23, no. 5, pp. 216–222, May 2000.

[28] B. Kang *et al.*, "Novel low-cost planar probes with broadside apertures for nondestructive dielectric measurement of biological materials at microwave frequencies," *IEEE Trans. Microw. Theory Techn.*, vol. 53, no. 1, pp. 134–143, Jan. 2005.

[29] K. Kwon *et al.*, "Planar type probe with multiple-polarization response for *in-vivo* permittivity measurements of heterogeneous biological tissues," *IEEE Microw. Wireless Compon. Lett.*, vol. 16, no. 1, pp. 1–3, Jan. 2006.

[30] N. Kim, J. Yoon, S. Cho, J. Cho, C. Cheon, and Y. Kwon, "An optimum design methodology for planar-type coaxial probes applicable to broad temperature permittivity measurements," *IEEE Trans. Microw. Theory Techn.*, vol. 56, no. 3, pp. 684–692, Mar. 2008.

[31] J. Muñoz-Enano, P. Vélez, M. Gil, and F. Martín, "Planar microwave resonant sensors: A review and recent developments," *Appl. Sci.*, vol. 10, no. 7, p. 2615, Apr. 2020.

[32] D. Ham and A. Hajimiri, "Concepts and methods in optimization of integrated LC VCOs," *IEEE J. Solid-State Circuits*, vol. 36, no. 6, pp. 896–909, Jun. 2001.

[33] Y. Kim and Y. Kwon, "Analysis and design of millimeter-wave power amplifier using stacked-FET structure," *IEEE Trans. Microw. Theory Techn.*, vol. 63, no. 2, pp. 691–702, Feb. 2015.

[34] R. S. Elliot, *Electromagnetics*. Hoboken, NJ, USA: Wiley, 1966, pp. 182–189. [Online]. Available: https://ieeexplore.ieee.org/book/5273681

[35] K. Shah, J. Sing, and A. Zayegh, "Modelling and analysis of fringing and metal thickness effects in MEMS parallel plate capacitors," *Proc. SPIE*, vol. 6035, Jan. 2006, Art. no. 603511.

[36] J. Hong and M. J. Lancaster, *Microstrip Filters for RF/Microwave Applications*. Hoboken, NJ, USA: Wiley, 2001, pp. 93–96. [Online]. Available: https://onlinelibrary.wiley.com/doi/book/10.1002/0471221619

[37] Y. Jin, J. Bae, and C. Nguyen, "A 4.6–5.9 GHz fully integrated 0.25-μm CMOS complementary LC VCO with buffer," in *Proc. 21st Int. Conf. Microw., Radar Wireless Commun. (MIKON)*, Krakow, Poland, May 2016, pp. 1–3.

[38] C.-C. Tu and C.-Y. Yang, "A 6.5-GHz LC VCO with integrated-transformer tuning," in *Proc. IEEE Asia–Pacific Conf. Circuits Syst. (APCCAS)*, Dec. 2006, pp. 510–513.

[39] M. Fathi, D. K. Su, and B. A. Wooley, "A stacked 6.5-GHz 29.6-dBm power amplifier in standard 65-nm CMOS," in *Proc. IEEE Custom Integr. Circuits Conf.*, Sep. 2010, pp. 1–4.

[40] M. A. Margarit, D. Shih, P. J. Sullivan, and F. Ortega, "A 5-GHz BiCMOS RFIC front-end for IEEE 802.11a/hiperLAN wireless LAN," *IEEE J. Solid-State Circuits*, vol. 38, no. 7, pp. 1284–1287, Jul. 2003.

[41] N. Kim, J. Yoon, C. Cheon, and Y. Kwon, "High-power reflection coefficient measurement of biological material applicable to microwave hyperthermia," in *IEEE MTT-S Int. Microw. Symp. Dig.*, Jun. 2009, pp. 1305–1308.

[42] D. Jung, Y. J. Hwang, H. Ryu, M. Kano, K. Sakimura, and J. Cho, "Conditional knockout of Cav2.1 disrupts the accuracy of spatial recognition of CA1 place cells and spatial/contextual recognition behavior," *Frontiers Behav. Neurosci.*, vol. 10, p. 214, Nov. 2016.

[43] E. J. Kim, E. S. Kim, M. Park, J. Cho, and J. J. Kim, "Amygdalar stimulation produces alterations on firing properties of hippocampal place cells," *J. Neurosci.*, vol. 32, no. 33, pp. 11424–11434, Aug. 2012.

[44] G. Arias-Gil, F. W. Ohl, K. Takagaki, and M. T. Lippert, "Measurement, modeling, and prediction of temperature rise due to optogenetic brain stimulation," *Neurophotonics*, vol. 3, no. 4, Oct. 2016, Art. no. 045007.

[45] W. Deng, E. M. Goldys, M. M. Farnham, and P. M. Pilowsky, "Optogenetics, the intersection between physics and neuroscience: Light stimulation of neurons in physiological conditions," *Amer. J. Physiol.-Regulatory, Integrative Comparative Physiol.*, vol. 307, no. 11, pp. R1292–R1302, Dec. 2014.

[46] S. Thomsen, "Pathologic analysis of photothermal and photomechanical effects of laser-tissue interactions," *Photochem. Photobiol.*, vol. 53, no. 6, pp. 825–835, Jun. 1991.

Seongwoog Oh (Graduate Student Member, IEEE) was born in Jeonju, South Korea, in 1995. He received the B.S. degree in electrical engineering and computer science from the Gwangju Institute of Science and Technology College, Gwangju, South Korea, in 2016, and the M.S. degree in electrical engineering from Seoul National University, Seoul, South Korea, where he is currently pursuing the Ph.D. degree in electrical engineering.

His current research interests concerned the design of microwave integrated circuits and systems for 5G communication and brain stimulation.

Dahee Jung was born in Seoul, South Korea, in 1987. She received the B.A. degree in life science from the University of Seoul, Seoul, and the Ph.D. degree in neuroscience from the University of Science and Technology, Seoul.

She is participating in project on the neuronal modulation via brain stimulation.

Taeyoon Seo (Member, IEEE) was born in Cheongju, South Korea, in 1981. He received the B.S. and M.S. degrees in electronics and information engineering from Korea Aerospace University, Gyeonggi, South Korea, in 2007 and 2010, respectively, and the Ph.D. degree in electrical engineering from Seoul National University, Seoul, South Korea.

He is currently working at Samsung Electronics Company Ltd., Suwon, South Korea. His research interests include computational electromagnetics, component design in microwave and millimeter-wave for bio-application.

Yeowool Huh was born in Busan, South Korea, in 1983. She received the B.A. degree in biological chemistry from Grinnell College, Grinnell, IA, USA, in 2005, and the Ph.D. degree in neuroscience from the University of Science and Technology, Daejeon, South Korea, in 2014.

She worked as a Post-Doctoral Researcher with the Korea Institute of Science and Technology, Seoul, South Korea, until 2017 and recently joined Catholic Kwandong University, International St. Mary's Hospital, Incheon, South Korea, as a Faculty Member. She is interested in understanding neural circuit-based mechanism of behavior and in brain stimulation.

Jeiwon Cho was born in Seoul, South Korea, in 1965. He received the B.A. degree in psychology from Yonsei University, Seoul, in 1990, and the M.S. and Ph.D. degrees in electrophysiology from Rutgers University, New Brunswick, NJ, USA, in 1994 and 1997, respectively.

He worked as a Post-Doctoral Researcher with the National Institute of Health, NIMH, Bethesda, MD, USA, from 1996 to 1997, Psychology, Yale University, New Haven, CT, USA, from 1997 to 1999, and University of California, Los Angeles, Brain Institute, Neurobiology, Los Angeles, CA, USA, from 1999 to 2001.

As a Principal Research Scientist, he worked in ChemOn Inc., Yongin, South Korea, from 2002 to 2003, in Seoul National University, Institute of New Media and Communications, Electrical Engineering, Seoul, from 2003 to 2006, and in Korea Institute of Science and Technology, Seoul, where he held a concurrent position as a Professor with the University of Science and Technology, Daejeon, South Korea, from 2006 to 2017. He was a Professor of medical science with Catholic Kwandong University, International St. Mary's Hospital, Incheon, Korea, and also a Deputy Director for the Institute for Biomedical Convergence, Incheon St. Mary's Hospital, from 2017 to 2020. Currently, he is a Professor of Brain and Cognitive Science, Scranton College, Ewha Womans University, Seoul, South Korea. He holds multiple patents on neural activity recording and stimulation devices.

Jungsuek Oh (Senior Member, IEEE) received the B.S. and M.S. degrees from Seoul National University, Seoul, South Korea, in 2002 and 2007, respectively, and the Ph.D. degree from the University of Michigan, Ann Arbor, MI, USA, in 2012.

From 2007 to 2008, he was with Korea Telecom, Seongnam, South Korea, as a Hardware Research Engineer, working on the development of flexible RF devices. In 2012, he was a Post-Doctoral Research Fellow with the Radiation Laboratory, University of Michigan. From 2013 to 2014, he was a Staff RF Engineer with Samsung Research America, Dallas, TX, USA, working as a Project Leader for the 5G/millimeter-wave antenna system. From 2015 to 2018, he was a Faculty Member with the Department of Electronic Engineering, Inha University, Incheon, South Korea. He is currently an Associate Professor with the School of Electrical and Computer Engineering, Seoul National University. His research areas include mmWave beam focusing/shaping techniques, antenna miniaturization for integrated systems, and radio propagation modeling for indoor scenarios.

Dr. Oh is the recipient of the 2011 Rackham Predoctoral Fellowship Award at the University of Michigan. He has authored more than 40 technical journal articles and conference papers, and has served as a technical reviewer for the IEEE TRANSACTIONS ON ANTENNAS AND PROPAGATION, IEEE ANTENNA AND WIRELESS PROPAGATION LETTERS, and so on. He has served as a Technical Program Committee (TPC) member and as a session chair for the IEEE Antennas and Propagation Society/US National Committee-Union of Radio Science (IEEE AP-S/USNC-URSI) and International Symposium on Antennas and Propagation (ISAP).